Using the lifetimes obtained above, the individual quenching rate constants k_q for the E and Z isomers of cyclooctene are calculated for the hexacarboxylates. As shown in Table IV, the quenching rate constants for (*E*)-cyclooctene, being fairly close to the diffusion rate constant, are 1.8–6.5 times greater than those for the Z isomer, probably owing to the much lower ionization potential[47,48] or singlet energy[49] of the E isomer. Significantly, the quenching rate constants for both E and Z isomers differ not only with the bulkiness of alkyl group but also with the excited state to be quenched, i.e., FC′ and RX, indicating that these two states bear considerable structural differences.

Acknowledgment. This work was supported in part by a Grant-in-Aid for Scientific Research (No. 63 550 630) from the Ministry of Science, Culture and Education of Japan, which is gratefully acknowledged.

(47) Batch, C.; Ermer, O.; Heilbronner, E.; Wiseman, J. R. *Angew. Chem.* **1973**, *85*, 302.
(48) Robin, M. B.; Taylor, G. N.; Kuebler, N. A. *J. Org. Chem.* **1973**, *38*, 1049.
(49) Sauers I.; Grezzo, L. A.; Staley, S. W.; Moore, J. H. *J. Am. Chem. Soc.* **1976**, *98*, 4218.

Study of Cu(II) Binding to Chiral Tripodal Ligands by Electron Spin Echo Spectroscopy

Daniella Goldfarb,*,† Jean-Michel Fauth,† Yitzhak Tor,‡ and Abraham Shanzer‡

Contribution from the Departments of Isotope Research and Organic Chemistry, The Weizmann Institute of Science, 76 100 Rehovot, Israel. *Received May 16, 1990*

Abstract: In an attempt to provide models for copper binding in proteins, symmetric and nonsymmetric chiral ligands designed to bind copper in a controlled geometry were synthesized. These ligands are assembled from trifunctional anchors extended by donors containing amino acids such as histidine and methionine. The copper coordination of these complexes was studied by orientation selective electron spin echo envelope modulation (ESEEM) experiments. The three-pulse FT-ESEEM spectra consist of peaks at 0.7, 1.4, 2.1, and 3.0 MHz, which positions are practically independent on the resonant magnetic field, and a peak at about 4 MHz, which shows significant field dependence. The relative intensities of all lines vary with the resonant field. These lines are typical for the remote nitrogen in the imidazole ring. By using computer simulations of the FT-ESEEM spectra recorded at the various resonant magnetic fields along the powder pattern and taking into account the selected excited orientations, the ^{14}N isotropic and anisotropic hyperfine interactions were determined. The simulations also gave the relative orientation of the ^{14}N hyperfine and quadrupole tensor principal axes with respect to the g tensor principal axis. From these parameters it was concluded that in the complexes consisting of three histidyl residues all three imidazoles are coordinated to the copper, not in a coplanar structure but in a propeller-like arrangement. No other nitrogens, such as the pivotal nitrogen, were found to be coordinated to the copper.

Introduction

Copper ions are found in the active sites of a number of important proteins and enzymes of vital biological functions.[1a-f] These proteins are associated with a variety of processes including oxygen transport, electron transfer, superoxide dismutation, hydrolytic reactions, and many more. Crystallographic and spectral studies of many copper-containing metalloproteins have unraveled the nature of the metallic binding sites. In many cases they were found to be rather simple and composed of three amino acids which are invariable throughout the catalytic process. Histidine imidazoles frequently occupy one or more of the coordination sites, together with cysteine and methionine sulfur donors, and less frequently aspartic acid and glutamic acid carboxylates. Extensive research efforts have been devoted to model the active sites of these proteins with simple, low molecular weight compounds that would simulate the coordinative environments present in the natural systems.[1b,g,h]

We have recently introduced novel families of chiral tripod-like ligands,[2] where the attachment of a bidentate ligand to each one of the tripodal arms affords octahedral biomimetic metal binders. The tripodal approach is eminently suited for modelling also tetrahedral and lower symmetry coordination sites. By attaching a monodentate ligand to each tripodal arm the invariable part of three essential donors is generated. In this article we present a novel type of symmetrical and nonsymmetrical tripodal ligands which possess the naturally occurring amino acids. These ligands are constructed from trifunctional anchors which are extended by donor containing chiral amino acids (e.g. histidine, methionine).

The extent of similarity between the synthetic models and natural proteins can be evaluated by comparing their spectral properties like ESR and electron spin echo envelope modulation (ESEEM) spectra.[3] ESEEM is particularly sensitive to the Cu(II) immediate environment since weak hyperfine interactions, normally hidden within the broad ESR line width, are easily detected. We thereby carried out a series of ESEEM experiments on the novel, tripodal ligand Tr(His)$_3$ (**1**) and its analogues, Ar(His)$_3$

† Department of Isotope Research.
‡ Department of Organic Chemistry.

(1) (a) Siegel H., Ed. *Metal Ions in Biological Systems*; Dekker: New York, 1981; Vol. 13, Copper Proteins. (b) Solomon E. I. In *Copper Coordination Chemistry: Biochemical and Inorganic Perspectives*; Karlin, K. D., Zubieta, J., Eds.; Adenine Press: New York, 1983; pp 1-22. (c) Solomon, E. I.; Penfield, K. W.; Wilkox, D. E. *Struct. Bonding* **1983**, *53*, 1-57. (d) Reinhammar, B. *Adv. Inorg. Biochem.* **1979**, *1*, 91-118. (e) Beinhert, H. *Coord. Chem. Rev.* **1980**, *33*, 55-85. (f) Fee, J. A. *Struct. Bonding* **1975**, *23*, 1-60. (g) Zobieta, J.; Karlin, K. D.; Hayes, J. C. In *Copper Coordination Chemistry: Biochemical and Inorganic Perspectives*; Karlin, K. D., Zubieta, J., Eds.; Adenine Press: New York, 1983; pp 97-108. (h) Urbach, F. L. *Metal Ions in Biological Systems*; Dekker: New York, 1981; Vol. 13, pp 73-115. (i) Sorrell, T. N. *Tetrahedron* **1989**, *45*, 3-68.
(2) (a) Tor, Y.; Libman, J.; Shanzer, A.; Lifson, S. *J. Am. Chem. Soc.* **1987**, *109*, 6517-6518. (b) Tor, Y.; Libman, J.; Shanzer, A. *J. Am. Chem. Soc.* **1987**, *109*, 6518-6519. (c) Libman, J.; Tor, Y.; Shanzer, A. *J. Am. Chem. Soc.* **1987**, *109*, 5880-5881. (d) Tor, Y.; Shanzer, A.; Scherz, A. *Inorg. Chem.* In press.
(3) Abbreviations used in the text; ESEEM, electron spin echo envelope modulation; NQR, nuclear quadrupole resonance; ENDOR, electron nuclear double resonance; LPSVD, linear prediction, singular value decomposition; Boc, *tert*-butoxycarbonyl; Tren, tris(2-aminoethyl)amine; CD, circular dichroism.

0002-7863/91/1513-1941$02.50/0

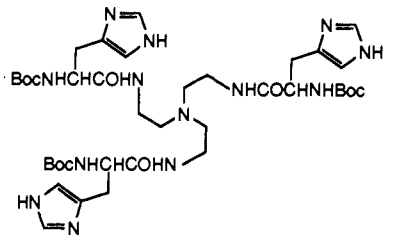

Tr(His)$_3$ **1**

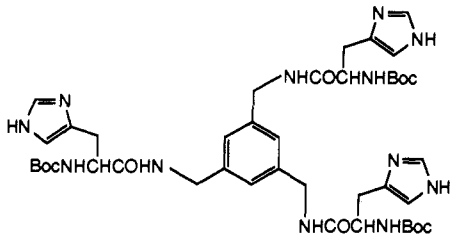

Ar(His)$_3$ **2**

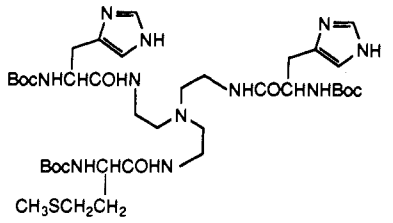

Tr(His)$_2$Met **3**

Boc = $(CH_3)_3C$-O-CO

Figure 1. The structure of the tripodal histidine ligands and their abbreviated names.

(**2**) and Tr(His)$_2$Met (**3**) (Figure 1). While Tr(His)$_3$ is based on tris(2-aminoethyl)amine (Tren) as anchor containing three histidyl residues, Ar(His)$_3$, lacks the pivotal nitrogen and Tr(His)$_2$Met contains merely two histidyl residues (see Figure 1).

ESEEM has been successfully applied in the past to the study of paramagnetic metalloproteins, as demonstrated by numerous publications by Mims, Peisach, and co-workers[4-9] and others.[11,12] When the binding involves an imidazole ring at an equatorial position the observed modulation is due to the remote nitrogen. In disordered samples, such as frozen solutions, when measured at 9 GHz the ESEEM displays several characteristic frequencies: two or three narrow lines at 0.5–2 MHz and a broader line at ~4 MHz.[6,9,12] The narrow low-frequency lines were assigned to the ^{14}N nuclear quadrupole resonance (NQR) frequencies which can be observed due to the so called "cancellation effect", where the effective field for one of the electronic submanifolds is close to zero. In this case the ^{14}N nuclear quadrupole coupling constant and the associated asymmetry parameter can be determined from the position of these lines. The isotropic hyperfine coupling constant is obtained from the position of the broad high-frequency line.[6-12]

In all above studies the ESEEM measurements were performed at a single resonant magnetic field, namely the field corresponding to the $g_\perp$ position. By performing field-dependent ESEEM measurements, i.e. changing the resonant field along the ESR powder pattern, information concerning the geometries of the complexes in question can be obtained and the isotropic hyperfine constant can be determined more accurately. Such orientation selective experiments are in principle similar to those performed in continuous wave ENDOR.[13] Reijerse et al.[14] demonstrated the applicability of field-dependent ESEEM experiments on Cu(II)-doped nickel(II) bis(*N*,*N*-diethyldithiocarbamate) in which all magnetic tensors have been previously determined by extensive single-crystal ESR, ESEEM, and ENDOR measurements. Flanagan et al.[15] used this approach to determine the orientation of the quadrupole interaction tensor of the imidazole's remote nitrogen in the mercaptoethanol complex of myloglobin. In this case the two-pulse ESEEM experiment was performed, yielding very broad lines, and the relative intensity of the NQR frequencies ν_+/ν_- was measured as a function of the resonant field. This ratio was then compared to that of simulated spectra. This analysis, however, did not include the anisotropic hyperfine interaction which may affect the relative intensities of the NQR lines.

In this article we demonstrate that by performing field-dependent three-pulse ESEEM measurements, following the dependence of both the ESEEM frequencies and their relative intensities, we were able to obtain information about the geometries of the tripodal Cu(II) complexes. Furthermore, we determined both the isotropic and the anisotropic hyperfine interactions.

Experimental Section

Synthesis of Histidine-Based Ligands. The detailed synthesis of the ligands is described elsewhere.[16] In the following we shall only briefly describe the procedure.

The tris-histidine ligands **1** and **2** have been prepared by activating DiBoc-L-histidine as *N*-hydroxysuccinimide active ester followed by coupling with tris(2-aminoethyl)amine or 1,3,5-tris(aminomethyl)-benzene, respectively. The N^{im}-Boc group was selectively removed by dilute sodium hydroxide followed by mild acidification ($KHSO_4$) to afford the protonated tris-histidine ligands. The preparation of ligand **3** bearing other donor-containing amino acids was performed by reacting Tren with a mixture of activated amino acids. Thus, reacting a mixture of *N*-hydroxysuccinimide activated esters of DiBoc-L-histidine and Boc-L-methionine with Tren affords a mixture of products of which the dominant ones were separated and found to be the protected Tr(His)$_2$Met (**3**). Deprotection was accomplished by similar basic hydrolysis.

Instrumentation. ESR measurements were performed on a Varian E-12 spectrometer at X-band (9.2 GHz) and spectra were recorded at 110 K. ESEEM experiments were performed at 4.2 K with a home built spectrometer. The structure of our spectrometer is generally similar to those described in the literature.[8,11,17] A tunable Gunn oscillator (MA/COM) is used as a microwave source (range 8.6–9.5 GHz). Microwave pulses are formed using a PIN diode switch (General Microwave) and their phase is controlled by a 2-bit digital-phase shifter (Vectronics). The pulses are amplified by a 1 KW TWT amplifier (Applied System Engineering). The detection system includes a limiter (Elisra) followed by a PIN diode switch (General Microwave), a high pass filter, a low noise amplifier (Miteq), and a double balanced mixer (RHG). The output signal is further amplified by an amplifier (DC-400 MHz, Stanford Research Systems, SR240) and is then fed into a boxcar gated integrator (Stanford Research Systems SR250) interfaced to a PC/AT computer via a DAS-8 board (Metrabyte) or by an SR245 computer interface unit (Stanford Research Systems).

The spectrometer is controlled by a pulse generator which consists of a 4 digital delay generators (Stanford Research Systems, DG535) ex-

(4) (a) Mims, W. B.; Peisach, J. In *Biological Magnetic Resonance*; Berliner, L. J., Reuben, J., Eds.; Plenum Press: New York, 1981; Vol. 3, pp 213–263. (b) Mims, W. B.; Peisach, J. In *Biological Applications of Magnetic Resonance*; Shulman, R. G., Ed.; Academic Press: New York, 1979; pp 221–269.
(5) Peisach, J.; Mims, W. B.; Davis, J. L. *J. Biol. Chem.* **1979**, *254*, 12379.
(6) Mims, W. B.; Peisach, J. *J. Biol. Chem.* **1979**, *254*, 4321.
(7) Avigliano, L.; Davis, J. L.; Graziani, M. T.; Marchesini, A.; Mims, W. B.; Mondovi, B.; Peisach, J. *FEBS Lett.* **1981**, *136*, 80.
(8) McCracken, J.; Peisach, J.; Dooley, D. M. *J. Am. Chem. Soc.* **1987**, *109*, 4064.
(9) McCracken, J.; Pember, S.; Benkovic, S. J.; Villafranca, J. J.; Miller, R. J.; Peisach, J. *J. Am. Chem. Soc.* **1988**, *110*, 1069.
(10) Jin, H.; Thomann, H.; Coyle, C. L.; Zumft, W. G. *J. Am. Chem. Soc.* **1989**, *111*, 4692.
(11) Britt, R. D.; Zimmermann, J. L.; Sauer, K.; Klein, M. P. *J. Am. Chem. Soc.* **1989**, *111*, 3522.
(12) Mims, W. B.; Peisach, J. *J. Chem. Phys.* **1978**, *69*, 4921.
(13) Hurst, G. C.; Henderson, T. A.; Kreilick, R. W. *J. Am. Chem. Soc.* **1985**, *107*, 7294.
(14) Reijerse, E. J.; van Earle, N. A. J. M.; Keijzers, C. P. *J. Magn. Reson.* **1986**, *67*, 114.
(15) Flanagan, H. L.; Gerfen, G. J.; Lai, A.; Singel, D. J. *J. Phys. Chem.* **1988**, *88*, 2162.
(16) Tor, Y. Ph.D. Thesis, Weizmann Institute of Science, Feb. 1990.
(17) Narayana, P. A.; Kevan, L. *Magn. Reson. Rev.* **1983**, *7*, 239.

Table I. Visible and CD Spectral Data of Cu(II) Complexes in Methanol

compd	λ_{max} (ϵ)	λ_{ext} ($\Delta\epsilon$)
$Tr(His)_3$ (**1**)	644 (81)	580 (−0.085)
$Ar(His)_3$ (**2**)	636 (71)	570 (+0.11)
$Tr(His)_2$ (**3**)	690 (80)	

ternally triggered by a pulse from the DAS-8 board and remotely controlled via GPIB interface (National Instruments) by the PC/AT computer.

The magnet used is part of the E-12 ESR spectrometer. The magnetic field was measured with a Bruker NMR Gaussmeter (ERO35 M) and the frequency was measured with a frequency counter (HP 5350B). The resonator employed was either an overcoupled TE_{102} cavity used with a liquid He glass dewar or a waveguide mounted folded half-wave resonator[18] designed to fit into the sample tube of a Janis 7.75 DT cryostat.

The ESEEMs were obtained by using the three-pulse sequence ($\pi/2$-τ-$\pi/2$-T-$\pi/2$-τ-echo) with phase cycling to eliminate unwanted echoes.[19] Typically, pulses of 20-ns duration were used with a power of about 40 W. The T incrementation was 10 or 20 ns.

Data Manipulation. To avoid distortions of the FT-ESEEM spectrum due to spectrometer dead time, typically τ + 40 ns for the three-pulse experiment, the missing data points were reconstructed using the linear prediction, singular value decomposition (LPSVD) method.[20] The background decay, due to relaxation, was removed by subtracting the appropriate zero-frequency component as obtained from the LPSVD procedure. Zero filling was then performed (up to a total of 1024 points) followed by Fourier transformation.

Results

Cu^{2+} Complexation. Treating a methanolic solution of the protonated tripodal histidine ligands with $CuCl_2$ and a weak base (CH_3COONa) afforded the light blue Cu(II) complexes. Their visible absorption and CD data are summarized in Table I. All the complexes exhibit a very broad absorption which tails into the infrared region, with λ_{max} in the range 640–690 nm, and relatively small molar extinction coefficients (70–80 M^{-1} cm^{-1}). The absorption maxima of these ligand field transitions are compatible with the coordination of Cu^{2+} to nitrogen imidazole donors and a possible one-oxygen donor.[4,21c] The mixed ligand containing His and Met exhibits a red-shifted absorption maxima, which is in agreement with a smaller number of coordinated nitrogens.[21] The similar λ_{max} strongly suggests that the *S*-methyl group is not coordinated to the Cu and is replaced by an oxygen donor. The relatively small extinction coefficients indicate the presence of complexes which are similar to normal (or type 2) copper proteins.

The visible CD spectra of the complexes are characterized by broad Cotton effects centered around 570 nm, with small $\Delta\epsilon$ values (Table I and Figure 2). Quite unexpectedly, the mesitylene and the Tren ligands show opposite Cotton effects. The similar visible spectrum which is accompanied by opposite CD spectra calls attention to similar coordination geometries but opposite helicites. This is supported also by the CD spectra in the UV region exhibiting a different pattern for the imidazole chromophores.[16]

The complex solutions were made with about 5% excess ligand. Accurate titration curves could not be obtained since the visible extinction coefficients of these complexes are small and rather close to the value obtained for the free copper salts. Accordingly a 4:3 ligand/Cu(II) ratio cannot be ruled out from these titrations; a 2:1 ratio is however definitely excluded. A 4:3 ratio would indicate an aggregate of 4 ligands and as will be discussed later we find this arrangement rather improbable.

ESR Measurements. The ESR spectra of Cu(II) complexes of **1**–**3** are shown in Figure 3. The spectra show ^{14}N superhyperfine splittings, at the $g_\perp$ region, with a separation of 15 G, which is typical for ^{14}N in histidine ligands.[21,22] The spin Hamiltonian parameters obtained for the complexes studied are listed in Table II. Since we could not observe the ^{14}N hyperfine splittings in the $g_\parallel$ region we did not attempt to evaluate $A_\parallel(^{14}N)$ and $A_\perp(^{14}N)$ from spectral simulations but accounted for it by increasing Gaussian line width. Note the reduction in the number

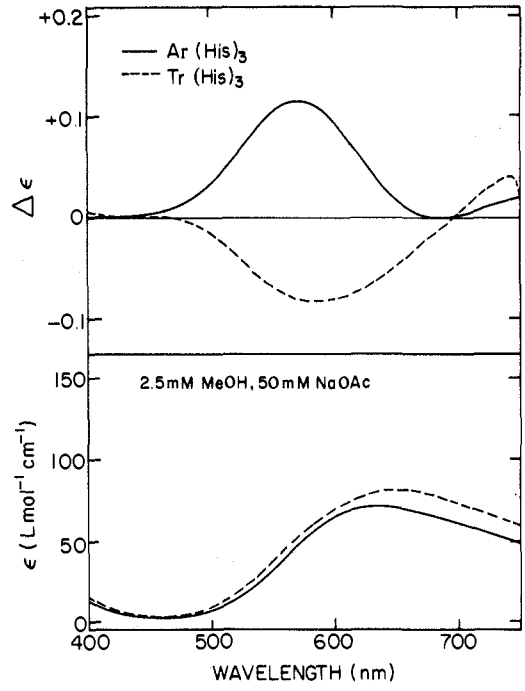

Figure 2. Visible and CD spectra of the Cu(II) complexes of ligands **1** (dashed line) and **2** (full line) in methanol.

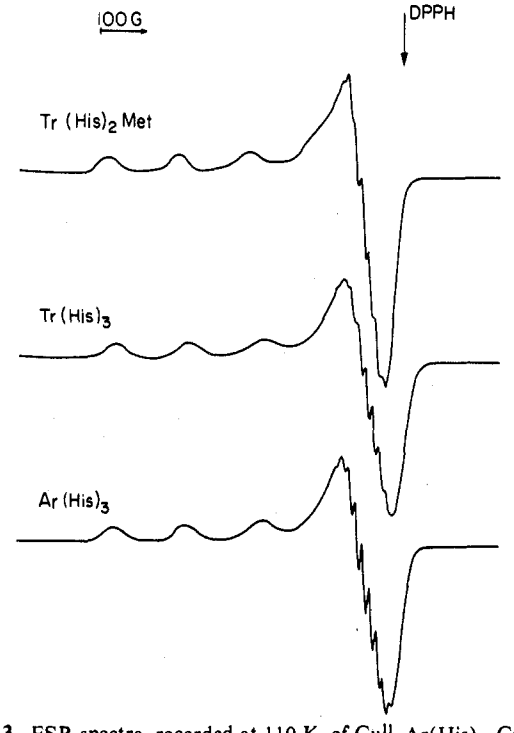

Figure 3. ESR spectra, recorded at 110 K, of Cu^{II}–$Ar(His)_3$, Cu^{II}–$Tr(His)_3$, and Cu^{II}–$Tr(His)_2Met$ in methanol solution (2.5 mM) in the presence of 50 mM $(CH_3COO)Na$.

(18) Britt, R. D.; Klein, M. P. *J. Magn. Reson.* **1987**, *74*, 535.
(19) Fauth, J.-M.; Schweiger, A.; Brauschweiler, L.; Forrer, J.; Ernst, R. R. *J. Magn. Reson.* **1986**, *66*, 74.
(20) Barkhuijsen, H.; de Beer, R.; Bovee, W. M. M. J.; van Ormondt, D. *J. Magn. Reson.* **1985**, *61*, 465.
(21) (a) Bernaducci, E.; Schwindinger, W. F.; Hughey, J. L., IV; Krogh-Jespersen, K.; Schugar, H. J. *J. Am. Chem. Soc.* **1981**, *103*, 1686–1691. (b) Bryce, G. F.; Gurd, F. R. N. *J. Biol. Chem.* **1966**, *241*, 122–129. (c) Sigel, H.; Martin, R. B. *Chem. Rev.* **1982**, *82*, 385–426.
(22) Arena, G.; Bonomo, R. P.; Impellizzeri, G.; Izatt, R. M.; Lamb, J. D.; Rizzarelli, E. *Inorg. Chem.* **1987**, *26*, 795.
(23) Traylor, T. G.; Hill, K. W.; Tiau, Z. Q.; Rheingold, A. L.; Peisach, J.; McCracken, J. *J. Am. Chem. Soc.* **1988**, *110*, 5571.

Table II. Spin Hamiltonian Parameters As Obtained from Simulations[a] of ESR Powder Patterns for Complexes 1-3

ligand	$g_{\parallel}$	$A_{\parallel}$(Cu), cm^{-1}	$g_{\perp}$	$A_{\perp}$(Cu), cm^{-1}
Ar(His)$_3$	2.271 ± 0.005	0.0178 ± 0.005	2.054 ± 0.005	0.00144 ± 0.0001
Tr(His)$_3$	2.271 ± 0.005	0.0178 ± 0.005	2.054 ± 0.005	0.00144 ± 0.0001
Tr(His)$_2$Met	2.306 ± 0.005	0.0172 ± 0.005	2.070 ± 0.005	0.00106 ± 0.0001

[a] The simulations did not include the superhyperfine interaction with the ^{14}N nuclei. We accounted for the broadening induced by this superhyperfine interaction by introducing an increasing Gaussian line width (50-60 G full width at half height).

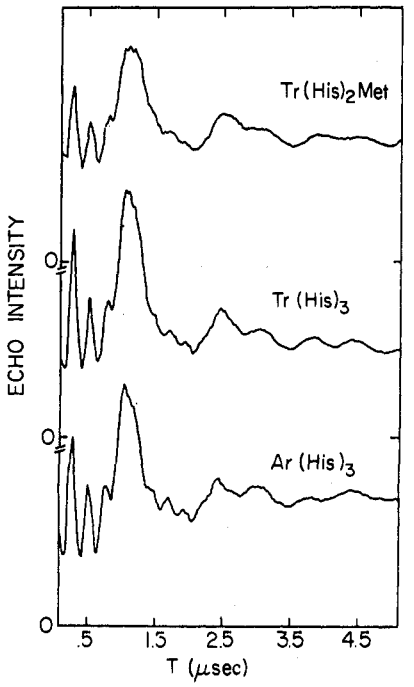

Figure 4. Three-pulse ESEEM, recorded at H = 3160 G, ν = 9.10 GHz and τ = 0.23 μs, of the three ligands studied.

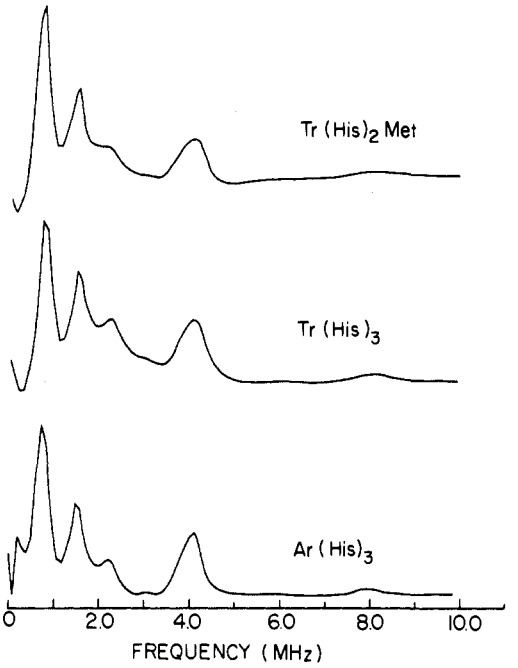

Figure 5. The cos FT-ESEEM spectra obtain from the time domain ESEEM shown in Figure 4.

and intensity of the ^{14}N superhyperfine lines in the spectrum of the Cu^{II}–Tr(His)$_2$Met which is consistent with binding to only two imidazole residues, compared to three in Cu^{II}–Tr(His)$_3$ and Cu^{II}–Ar(His)$_3$. A more diluted (1 mM) solution of Cu^{II}–Tr(His)$_3$ showed somewhat better resolution in the $g_{\perp}$ region.

ESEEM Measurements. The three-pulse ESEEM of complexes **1-3**, recorded at the field position where the echo intensity was a maximum (denoted as $g_{\perp}$) with τ = 0.23 μs, are shown in Figure 4, and the corresponding FT-ESEEM spectra are shown in Figure 5. All spectra exhibit lines at 0.7, 1.46, 2.2, 3.0, 4.1, and 8.0 MHz which were assigned to the remote nitrogen of the imidazole ring based on the work of Mims and Peisach.[12] The lines at 0.7 and 1.46 MHz correspond to the NQR frequencies of the remote imidazole nitrogen, and the 2.2-, 3.0-, and 8.0-MHz peaks are combination frequencies arising from interaction with several ^{14}N nuclei.[9] The intensities of these lines are stronger in Cu^{II}–Ar(His)$_3$ and Cu^{II}–Tr(His)$_3$ as compared to Cu^{II}–Tr(His)$_2$Met since in the later only two identical ^{14}N are involved in the modulation whereas in the former complexes three ^{14}N nuclei are involved.[9] The ESEEM of all three complexes recorded with τ = 0.18 μs, keeping the resonant field and spectrometer frequency constant, exhibited the same frequencies as those observed with τ = 0.23 μs. The relative intensities of the combination peaks and of the 4-MHz line were, however, somewhat stronger. A significant reduction in the intensity of the combination peaks in Cu^{II}–Tr(His)$_2$Met as compared to Cu^{II}–Ar(His)$_3$ and Cu^{II}–Tr(His)$_3$ was observed as well.

The ESEEM of Cu^{II}–Ar(His)$_3$ and Cu^{II}–Tr(His)$_3$ were measured at several field positions for two τ values, 0.22 and 0.30 μs. The spectra obtained for τ = 3.0 μs are shown in Figure 6. Note that the positions of all lines, besides the high-frequency lines at ~4 and ~8 MHz, are essentially field independent, indicating that throughout the field range measured the cancellation effect is significant. The relative intensities of these lines, however, do change. The position of the ~4-MHz line increases with increasing magnetic field; furthermore, it is significantly narrower when measured at low fields.

Table III. The Isotropic Hyperfine Constant Calculated with Equation 1 for K = 0.35 MHz and η = 1 as a Function of the Resonant Field for Cu^{II}–Tr(His)$_3$ (τ = 0.22 μs)

field, G	ν_1, MHz	$2\nu_m$, MHz	a_{iso}, MHz
3225	0.99	4.05	1.82
3120	0.96	4.00	1.82
2901	0.89	3.71	1.65
2767	0.85	3.53	1.54
2678	0.82	3.50	1.55

The field dependence of the ESEEM frequencies and their relative intensities (taking the intensity of the line at 0.7 MHz as 1.0) for Cu^{II}–Tr(His)$_3$ at τ = 0.22 μs are summarized in Figures 7 and 8. It should be noted that the relative intensities, in particular that of the 4-MHz line, have larger uncertainties than the frequencies due to the dead time reconstruction.

Spectral Analysis and Simulations. The magnetic field independence of the low-frequency lines supports their assignment to the NQR frequencies of the remote nitrogen in the imidazole ring.[12] Close observation of Figures 5 and 6 reveals that the line at 0.7 MHz is somewhat broader than the line at 1.46 MHz suggesting that the asymmetry parameter of the ^{14}N nuclear quadrupole tensor, η, is slightly smaller than 1. Ignoring this difference and taking η = 1 and (e^2qQ_N/h) = 1.4 MHz we obtain NQR frequencies at 0.7 and 1.4 MHz which agree with our measured values. Assuming that the anisotropic hyperfine is negligible, the isotropic hyperfine interaction, a_{iso}, can be calculated from the high-frequency line (~4 MHz), $2\nu_m$, according to[24]

$$\nu_m = (\nu_{ef}^2 + K^2(3 + \eta^2))^{1/2} \quad (1)$$

(24) Dikanov, S. A.; Astashkin, Yu. D.; Goldfeld, H. G. *Chem. Phys. Lett.* **1983**, *101*, 206.

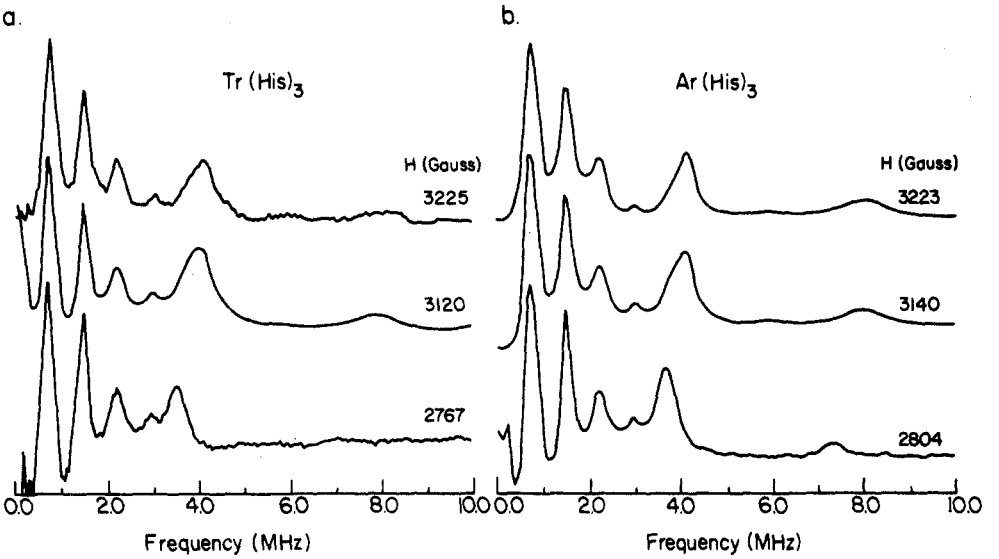

Figure 6. cos FT-ESEEM spectra of (a) Cu^{II}–Tr(His)$_3$ and (b) Cu^{II}–Ar(His)$_3$ recorded at various resonant magnetic fields (τ = 0.3 μs) at frequencies of 9.021 and 9.043 GHz, respectively.

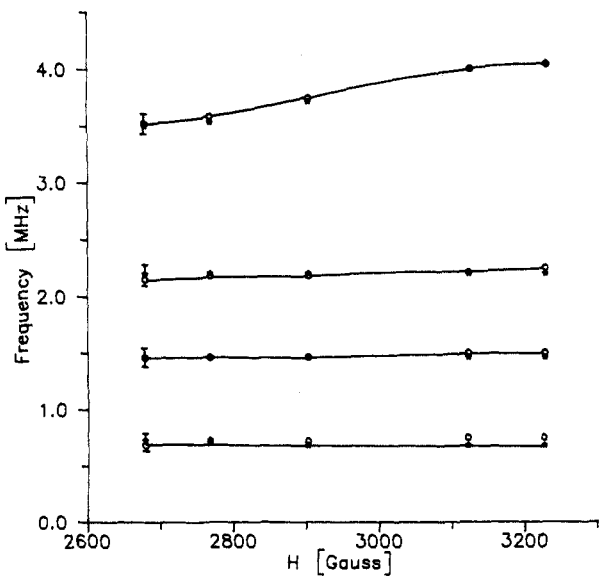

Figure 7. The field dependence of the FT-ESEEM frequencies of Cu^{2+}–Tr(His)$_3$ (τ = 0.22 μs; ν = 9.021 GHz): (*) experimental, (O) calculated.

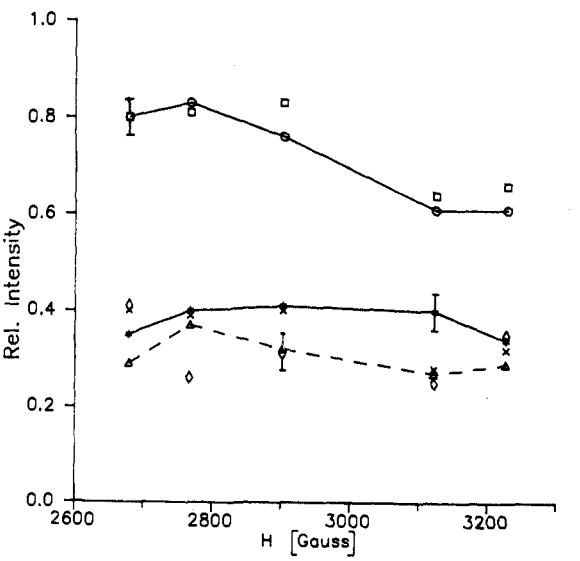

Figure 8. The field dependence of the relative intensities of the FT-ESEEM peak of Cu^{II}–Tr(His)$_3$ (τ = 0.22 μs; ν = 9.091 GHz): (O, *, and Δ) experimental points; (□, X, and ◇) calculated points.

where $K = e^2qQ_N/4h$, ν_{ef} is the effective nuclear frequency and is given by $\nu_{ef} = |\nu_1 \pm {}^1/_2 a_{iso}|$, and ν_1 is the nuclear Larmor frequency at the applied magnetic field. Using eq 1 and the measured $2\nu_m$ frequencies we calculated a_{iso} for each magnetic field position (Table III). The variation of a_{iso} as a function of the magnetic field indicates that in this case the $2\nu_m$ frequency does not solely depend on the Zeeman, quadrupole, and isotropic hyperfine interactions but is affected by the anisotropic hyperfine interaction as well. The effect of the anisotropic hyperfine interaction on the position of the high-frequency line has already been shown by Reijerse et al.[25]

In light of these results, we carried out computer simulations of the ESEEM recorded at the various resonant fields and both the g anisotropy and the anisotropic hyperfine interactions were taken into consideration.

Our calculations are essentially similar to those we previously described[26,27] where we followed the approach of Rowan et al.[28] for introducing the g anisotropy in the calculation of the echo intensity. Neglecting the hyperfine and quadrupole interactions of the copper nucleus, which do not affect the ESEEM,[28,29] the spin Hamiltonian, expressed in the **g** tensor principal axis system, is given by

$$H_T = (\beta/h)H\cdot\mathbf{g}\cdot S - (g_n\beta_n/h)H\cdot I + I\cdot\mathbf{A}'\cdot S + I\cdot\mathbf{Q}\cdot I \quad (2)$$

The Euler angles α, β, and γ relate the principal axis systems of the **Q** and **g** tensors.[30] The hyperfine tensor **A**′ in eq 1 is defined as

$$\mathbf{A}' = (A_{iso}\mathbf{1} + \mathbf{A})\cdot\mathbf{g} \quad (3)$$

where for isotropic g, $a_{iso} = gA_{iso}$. The polar angle θ_1 and the corresponding azimuthal angle ϕ_1 relate the **A** and **g** tensors principal axis systems. The diagonal elements of the **A** tensor (taken as axially asymmetric) in its principal frame are $2A_\perp$, $-A_\perp$, and $-A_\perp$. θ_0 is the angle between the applied magnetic field and the **g** tensor principal axis, z, and ϕ_0 is the corresponding azimuthal angle. By making the standard transformation, defining g_{ef},[31,32]

(25) Reijerse, E. J.; Keijzers, C. P. *J. Magn. Reson.* **1987**, *71*, 83.
(26) Goldfarb, D.; Kevan, L. *J. Chem. Phys.* **1987**, *87*, 6323.
(27) Goldfarb, D.; Kevan, L. *J. Magn. Reson.* **1989**, *82*, 270.
(28) Rowan, L. G.; Hahn, E. L.; Mims, W. B. *Phys. Rev. A* **1965**, *137*, 61.
(29) Mims, W. B. *Phys. Rev. B* **1972**, *5*, 2409; **1973**, *6*, 3543.
(30) The quadrupole tensor in its principal axis system is given by the following: $Q^p_{zz} = Q/2I(2I-1)$; $Q^p_{xx} = -Q^p_{zz}(1-\eta)/2.0$; $Q^p_{yy} = -Q^p_{zz}(1+\eta)/2.0$.
(31) $g^2_{ef} = g^2_\parallel \cos^2\theta_0 + g^2_\perp \sin^2\theta_0$.

Table IV. The μ_i and σ_i Used for Calculating the Orientations, θ_0, Contributing to the Echo for Each m_I(Cu) (See Equation 6 and Figure 10)

	m_I(Cu)							
	$^3/_2$		$^1/_2$		$-^1/_2$		$-^3/_2$	
field, G	μ, deg	σ,[a] deg	μ, deg	σ, deg	μ, deg	σ, deg	μ, deg	σ, deg
2678	31.0	7.0						
2763	43.0	7.0	12.0	14.0				
2901	61.0	5.0	43.0	8.0				
3120	90	7.0	83.0	9.0	62.0	14.0	16.0	16.0
3225							66.0	15.0

[a] $\sigma = \Gamma/2.35$, where Γ is the full line width at half height.

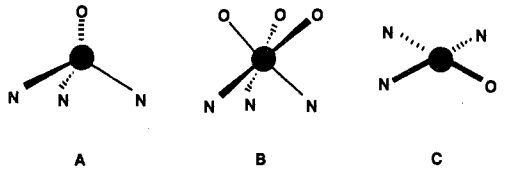

Figure 9. A schematic illustration of the three structures examined (N corresponds to the bound nitrogen).

and neglecting terms off diagonal in S (such as I_iS_j where $i = x, y, z$ and $j = x, y$), H_T becomes diagonal in S.[28,29]

Following these manipulations H_T is broken into two blocks representing two nuclear Hamiltonians, each corresponding to one of the $M_s = \pm^1/_2$ electronic states, and Mims' general expressions can be used to calculate the ESEEM.[29] The eigenvalues and the eigenvectors of the above two nuclear Hamiltonians were obtained by numerical diagonalization, though analytical expressions are available for $I = 1$.[33]

In both Cu^{II}–$Tr(His)_3$ and Cu^{II}–$Ar(His)_3$ the ESEEM is induced by three identical ^{14}N nuclei and the total modulation is obtained from[34]

$$E(\tau,T,\theta_0,\phi_0) = \frac{1}{2}\{\prod_{i=1}^{3} E_i^{\alpha}(\tau,T,\theta_0,\phi_0) + \prod_{i=1}^{3} E_i^{\beta}(\tau,T,\theta_0,\phi_0)\} \quad (4)$$

where $E_i^{\alpha,\beta}$ represents the modulation due to nucleus i, $i = 1, 2$, or 3 and α and β refer to the different electronic manifolds. Since three different tensors are involved, $\mathbf{g}$, $\mathbf{A}'$, and $\mathbf{Q}$, the powder integration should be performed over two angles θ_0 and ϕ_0. For convenience we chose our axis system such that ϕ_0 is nonzero and the Euler angles ϕ_I and γ are ϕ_0 dependent as described later on.

We considered two types of structures, which are schematically shown in Figure 9A–C. In the first structure the three nitrogens are arranged in a trigonal symmetry about the Cu(II). In this case A_{iso}, $A_\perp$, θ_I, K, η, and β are similar for all three nitrogens and the ϕ_{1i} and γ_i are correlated as follows:

$$\phi_{1i} = \phi_{11} + x(i-1);\ \gamma_i = \gamma_1 + x(i-1) \quad (5)$$

where $i = 2$, 3 and $x = (2\pi/3)$. Since H is not restricted to the xz plane the angles ϕ_I and γ should be replaced by $\phi_I' = \phi_I - \phi_0$ and $\gamma' = \gamma - \phi_0$.[26,28] This structure fits an octahedral arrangement of ligands with a trigonal distortion, involving the three imidazole residues and the three oxygenous ligands such as acetate and/or methanol. Another possibility is a tetrahedral arrangement of ligands, three imidazoles and one oxygenous ligand.

The second type is a square-planar or a square-pyramidal arrangement. In this case three of the four equatorial ligands are nitrogenous; the fourth ligand and the additional axial ligand are again oxygenous ligands. In this case eq 5 holds with $x = (\pi/2)$.

Due to the large g anisotropy and to the limited power of the microwave pulse, at each resonant field, only selected orientations are excited and contribute to the echo intensity. With use of the ESR parameters $g_\parallel$, $g_\perp$, $A_\parallel$(Cu), and $A_\perp$(Cu) (see Table II), a plot of the resonant magnetic field for each m_I(Cu) value as function of θ_0 was generated (Figure 10). The orientations contributing to the echo intensity for each experimental resonant field were determined graphically from this plot. To account for the inhomogeneous line width, which includes the bound ^{14}N-hyperfine splittings, and for the spectral width of the applied pulse, integration was performed over a range of θ_0.[14] A total line width of 60 G was taken, represented as dashed lines in Figure 10, from which the integration range over θ_0 was estimated.

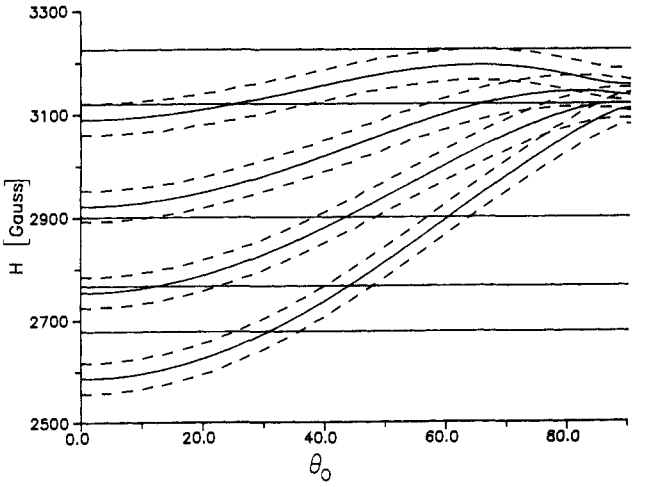

Figure 10. Plot of the resonance field for each m_I(Cu) state as a function of the orientation of the local symmetry axis with respect to the external magnetic field, θ_0.

Table V. The Parameters Used for the Simulation

$g_\parallel = 2.271$	$\phi_I = 0°$
$g_\perp = 2.054$	$e^2qQ/h = 4K = 1.45$ MHz
$A_{iso} = 0.71$ MHz	$\eta = 0.9$
$A_\perp = 0.11$ MHz	$\beta = 40°$
$\theta_I = 80°$	$\alpha = \gamma = 0°$

The total echo intensity was calculated from

$$E(\tau,T,H) = \sum_{i=1}^{4} \frac{1}{\sigma_i\sqrt{2\pi}} \int_0^{\pi} \int_{\mu_i-2\sigma_i}^{\mu_i+2\sigma_i} E(\tau,T,H,\theta_0,\phi_0) e^{-\frac{1}{2}(\theta_0-\mu_i)/\sigma_i|^2} \sin\theta_0\, d\theta_0\, d\phi_0 \quad (6)$$

The above expression includes a Gaussian weighting function. The summation is over the four m_I(Cu) values, and Table IV lists the various σ_i and μ_i used in the calculation for each resonant field.

The parameters involved in the simulations are the following: A_{iso}, $A_\perp$, θ_I, ϕ_I, K, η, α, β, and γ. K and η can be determined from the low-frequency lines thus leaving five unknown parameters. In finding the best-fit parameters we followed the procedure suggested by McCracken et al.[9] with some modification since they did not take into account the g anisotropy, and measurements were performed at a single resonant field, namely the $g_\perp$ position. We found that the $2\nu_m$ frequency is mostly affected by A_{iso}, $A_\perp$, and θ_I, where we limited θ_I to the range 60–120 °C due to steric considerations. We made a series of plots, where the position of $2\nu_m$ was calculated for several values of θ_I as a function of A_{iso} and of $A_\perp$, for the two extreme resonant fields (2678 and 3120

(32) Atherton, N. M. *Electron Spin Resonance, Theory and Application*; John Wiley and Sons, Inc.: New York, 1973; p 223.
(33) Bowman, M. K.; Massoth, R. J. In *Electronic Magnetic Resonance of the Solid State*; Weil, J. M., Ed.; Canadian Society of Chemistry: Ottawa, 1987; p 99.
(34) Dikanov, S. A.; Shubin, A. A.; Parmon, V. N. *J. Magn. Reson.* **1981**, *42*, 474.

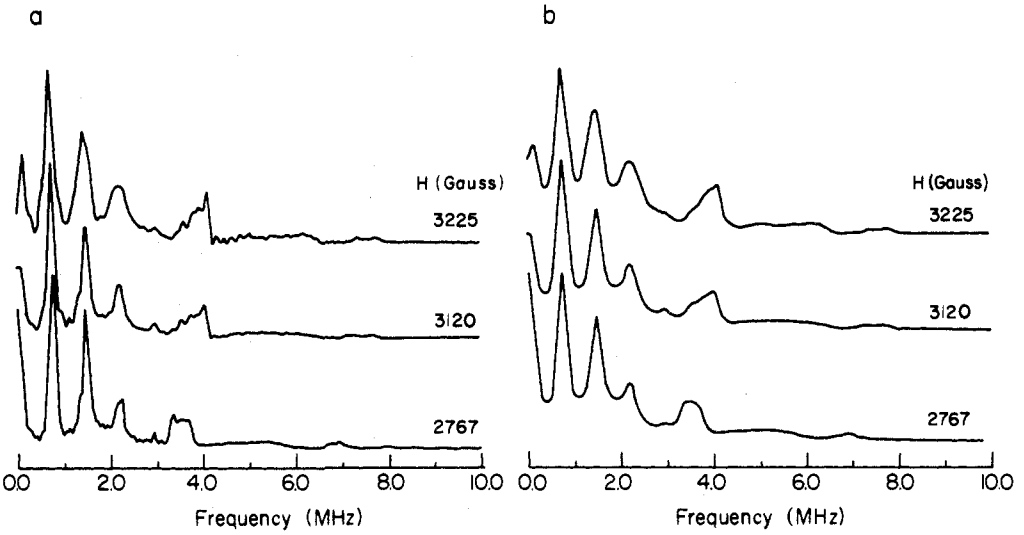

Figure 11. Computer simulation of three pulse FT-ESEEM spectra as a function of resonant field for $\tau = 0.3$ μs obtained with the parameters listed in Table V with line broadening $e^{-(T+\tau)/t_0}$: (a) $t_0 = 10$ μs; (b) $t_0 = 2$ μs. The parameters involved in the integration are given in Table IV.

G). Using these plots we could get a good estimate for these three parameters. The next parameter considered was β which has a considerable effect on the intensity of the $2\nu_m$ line, not necessarily similar at the low and high resonant fields. The last parameters α, ϕ_1, and γ affect mostly the line shape of the high-frequency line and to some extent the relative intensities of the NQR lines.

We found that the calculated ESEEM traces were not very sensitive to the two structures with $x = \pi/2$ and $2\pi/3$ discussed above. This is not surprising considering the powder overaging. The differences were manifested mainly in the line shape of the $2\nu_m$ line; such differences are far beyond our experimental error.

Using the parameters listed in Table V we could rather satisfactorily reproduce the positions of all lines, four of which are shown in Figure 7. The corresponding calculated relative intensities as compared to the experimental intensities are shown in Figure 8. In this case the relative intensities of the two strong lines at 0.7 and 1.46 MHz show a reasonable agreement whereas larger deviations are observed for the 2.2- and 4-MHz lines. Nonetheless, the deviation is tolerable considering the experimental uncertainty introduced by the dead time.

Figure 11 shows the calculated FT-ESEEM spectra with $\tau = 0.3$ μs (to be compared with Figure 6). In Figure 11a the calculated ESEEM traces were multiplied by $e^{-(T+\tau)/t_0}$ with $t_0 = 10$ μs to account for the spin relaxation, and the "noise" is due to truncation of the ESEEM before the modulation has decayed to zero. The width of the low-frequency lines is still narrower than in the experimental results. Multiplication by a decaying exponent with $t_0 = 2.0$ μs yields the spectra shown in Figure 11b which show a better agreement with the experimental results. Note that the calculated spectra reproduce the increase in the line width of the $2\nu_m$ line with increasing resonant field. This is expected for the case where the ligands are in a plane approximately perpendicular to the $g_\parallel$ direction. When the magnetic field is in the xy plane ($g_\perp$ position) all the orientations with different ϕ_0 exhibit different anisotropic hyperfine interactions and thus contribute to the broadening of the line. The variation in the line width of the other lines is reproduced as well. The relative intensity of the $2\nu_m$ line, however, is weaker than that in the experimental spectra. It could be increased by increasing A_{iso} and decreasing $A_\perp$, but by introducing such a change we could not reproduce the frequency change of this line as a function of the field.

Discussion

The binding of the copper to the imidazole rings is evident from both the ESR and ESEEM measurements. The ESR spectra showed ^{14}N superhyperfine splittings and the $g_\parallel$, $g_\perp$, $A_\parallel$(Cu), and $A_\perp$(Cu) of the three Cu(II) complexes studied are typical of Cu(II) complexes with imidazole rings.[22,23,35-37] The ESEEM frequencies of all three complexes studied are characteristic of the remote nitrogen in the imidazole ring and were previously observed in a number of metalloproteins such as stellacyanine,[6] porcine kidney amine oxidase,[8] laccase,[7] cytochrome P-450,[5] and dopamine β-hydroxylase.[35]

The relative intensities of the combination peaks in the FT-ESEEM spectra of Cu^{II}–$Tr(His)_3$ and Cu^{II}–$Ar(His)_3$ complexes agree well with three equivalent ^{14}N nuclei being involved in the modulation. As expected, the intensities of these peaks in Cu^{II}–$Tr(His)_2Met$ are reduced since the ligand consists of only two imidazoles. This is further supported by the decrease in the number of superhyperfine lines in the corresponding ESR spectrum. The increase in $g_\parallel$ and the slight decrease of $A_\parallel$(Cu) in Cu^{II}–$Tr(His)_2Met$, as compared to the other two complexes, are consistent with the replacement of one of the nitrogenous ligands with an oxygenous ligand and not with coordination to sulfur.[36] This is in line with the red-shifted absorption maximum of Cu^{II}–$Tr(His)_2Met$ mentioned above. Cu^{II}–$Tr(His)_3$ and Cu^{II}–$Ar(His)_3$ exhibit practically identical ESR and ESEEM spectra; since the later lacks any N in the anchor, we conclude that the Cu^{II} in Cu^{II}–$Tr(His)_3$ is not bound to the pivotal nitrogen. Again, their similar absorption maxima which indicate a similar coordinated donor support this conclusion.

The ESEEM of Cu(II) in dopamine β-hydroxylase measured at $g_\perp$ is very similar to that of Cu^{II}–$Tr(His)_3$ and Cu^{II}–$Ar(His)_3$; the only significant difference is the splitting in the 4-MHz line.[35] In this case the ESEEM was interpreted, based on computer simulations at only one resonant field, in terms of interactions with four imidazoles divided into two sets with different coupling parameters. The authors stated, however, that the choice between three or four bound imidazoles cannot be made with certainty. Interaction with four imidazoles with identical magnetic parameters gave combination peaks considerably stronger than those observed in our results.[9,23,35] Considering the structure of our ligands and the titration results, coordination to four imidazoles would mean a 4:3 ligand/Cu(II) ratio and not a 2:1 ligand/Cu(II) ratio. This implies a cluster of 3 Cu^{2+} and 4 ligands. In such a cluster the Cu(II)–Cu(II) distances are relatively short and spin–spin interactions become significant, thus reducing T_2 and the echo intensity. We did not observe any significant decrease in echo intensity as compared to similar solutions without the ligand. Furthermore if such aggregates are formed then in the $Tr(His)_2Met$ ligand one would expect three imidazoles to be coordinated to each Cu(II). Our experimental results disagree with this possibility since the combination peaks are too weak and the ESR spectrum does not show enough ^{14}N superhyperfine lines.

(35) McCracken, J.; Descu, P. R.; Papadopoulos, N. J.; Villafranca, J. J.; Peisach, J. *Biochemistry* **1988**, *27*, 4133.
(36) Peisach, J.; Blumberg, W. E. *Arch. Biochem. Biophys.* **1974**, *165*, 691.

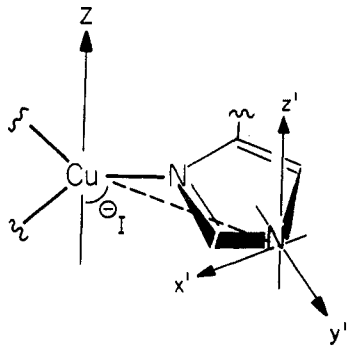

Figure 12. The coordinate system and the angles used in the simulations with respect to the molecular structure. The z axis represents the local symmetry axis of the complex, coinciding with the $g_{\parallel}$ direction. The x', y', and z' axes correspond to the principal system of the ^{14}N quadrupole tensor, and β is the angle between z and z'. θ_1 is the angle between the z axis and the vector connecting the Cu(II) and the remote nitrogen.

On the basis of the above considerations we fitted the ESEEM results of Cu^{II}–$Tr(His)_3$ and Cu^{II}–$Ar(His)_3$ to Cu^{II} coordinated to three equivalent imidazoles, which is also the most probable arrangement, taking into account the highly symmetric structure of the ligands.

As mentioned earlier we considered three possible structures for the complexes of Cu(II) with $Tr(His)_3$ and $Ar(His)_3$, as shown in Figure 9: (a) tetrahedron, (b) octahedron with a trigonal distortion, and (c) square planar or square pyramidal. All structures involve three nitrogenous donors, and the rest of the ligands are oxygenous, i.e. methanol and/or acetate. We did not consider an octahedron with a tetragonal distortion since there is no space for a ligand between the anchoring moiety connecting the three peptides and the copper cation.

The values of $\beta = 40°$ and $\theta_1 = 80°$, obtained from the simulations, rule out the possibility of the imidazole rings being coplanar. Taking into account that the principal component of the electric field gradient tensor of the remote ^{14}N is close to the perpendicular to the ring plane and that the other two axes are along the CNC bisector and the tangential to the ring respectively[37] (as shown in Figure 12) implies that β should be close to zero for a coplanar structure. Furthermore, assuming that the anisotropic hyperfine interaction is mainly dipolar in nature, thus placing its principal axis parallel to the vector connecting the remote ^{14}N nucleus and the copper cation (see Figure 12), a coplanar structure should give $\theta_1 = 90°$. To afford the values $\beta = 40°$ and $\theta_1 = 80°$ the imidazole rings must be rotated away from the plane creating a propeller-like structure.

Although the angles β and θ_1 we found are consistent with a distorted tetrahedral structure, (a), such an arrangement has to be ruled out since the $A_{\parallel}(Cu)$ observed is too large.[36,38] This leaves possibilities (b) and (c); the value $\theta_1 = 80°$ agrees better with structure (b), which is also more favorable considering the symmetry of the tripodal ligand.[39]

Further support for the octahedral arrangement with a trigonal distortion is obtained by comparison with the data reported by Laussac et al.[40] These authors reported, for the complexation of Cu(II) with a macrocyclic peptide, containing tris-histidyl residues, values of $A_{\parallel}(Cu) = 0.00183$ cm^{-1} (174 G), $g_{\parallel} = 2.252$, and $g_{\perp} = 2.060$, which are very close to our values.

From the ESEEM simulations we found that $A_{iso} = 0.71$ MHz and $A_{\perp} = 0.11$ MHz. In order to compare them to values obtained from other complexes where the g anisotropy was not taken into account, these values should be multiplied by $g \sim 2$ yielding $a_{iso} = 1.42$ MHz and $a_{\perp} = 0.22$ MHz. The value 1.42 MHz is smaller than the 1.8 MHz obtained for porcine kidney amine oxidase[8] and other Cu^{II}–imidazole complexes[10] which exhibit, when recorded at the $g_{\perp}$ position, peaks at 0.7, 1.4, and 4.0 MHz, as in our measurements. In the latter cases a_{iso} was determined from measurements performed at only one resonant field and contributions from the anisotropic hyperfine interaction were neglected, thus included in a_{iso}. We could obtain a good fit for the ESEEM frequencies, recorded at the $g_{\perp}$ position with $a_{iso} = 1.8$ MHz, but the frequencies obtained at low resonant fields could not be fitted with the same parameters. The constraints obtained by measuring the ESEEM at several resonant fields enabled a refinement of the isotropic hyperfine constant and the determination of the anisotropic hyperfine interaction which was found to affect the ESEEM frequencies, their width, and their relative intensities.

Although the parameters determined through the simulations may not be unique, the deviation range of A_{iso}, $A_{\perp}$, and θ_1 is not more than 10%; a somewhat broader span exists for β, whereas large variations are expected for the angles α, ϕ_1, and γ.

As mentioned in the previous section we could not account for the whole line width by considering only the appropriate orientation averaging and the background decay due to electronic spin relaxation. We do not know the origin of this additional broadening; it could be due to some distribution in the parameters involved, such as θ_1 and β, which may be possible if in solution rotation about the Cu^{II}–N axis is exercised. Another possibility is that the three nitrogens are not fully equivalent such that they have slightly different parameters. This could explain the line width differences in the $2\nu_m$ line in Cu^{II}–$Tr(His)_3$ and Cu^{II}–$Ar(His)_3$. It should be noted that McCracken et al.[9] also had to introduce a rather large line broadening (2.4 μs), not expected from the experimental background decay, to fit the experimental ESEEM spectra of phenylalanine hydroxylase.

Conclusions

Through ESR and field dependent ESEEM measurements we were able to obtain the following structural information regarding the binding of Cu(II) to the novel synthetic tripodal ligands $Tr(His)_3$, $Ar(His)_3$, and $Tr(His)_2Met$: (a) In Cu^{II}–$Tr(His)_3$ and Cu^{II}–$Ar(His)_3$ the Cu(II) is coordinated to three imidazoyl rings whereas in Cu^{II}–$Tr(His)_2Met$ it is coordinated only to two imidazoyl rings. (b) The pivotal nitrogen in Cu^{II}–$Tr(His)_3$ is not coordinated to the Cu(II). (c) The binding site in Cu^{II}–$Tr(His)_3$ and Cu^{II}–$Ar(His)_3$ has an octahedral geometry with a trigonal distortion and the imidazoyl rings forming a propeller-like arrangement.

Study of both naturally occurring copper binding sites in proteins and in synthetic models, designed to simulate metal binding sites in proteins, by field dependent ESEEM measurements is anticipated to provide detailed information on the structural features of the copper centers and to possibly allow differentiation of subtle variations, which might be relevant to the activity of these compounds.

Acknowledgment. This study was made possible (in part) by funds granted to D.G. through a fellowship program sponsored by the Charles H. Revson Foundation. Additional support was given by the Bat-Sheva de Rothschild Foundation for the Advancement of Science and Technology. The help of Y. Gorodetzki, Y. Zibziner, and Y. Lipkin in the construction of the pulsed ESR spectrometer is greatly acknowledged and so is helpful advice from L. Kevan, H. Thomann, A. Schweiger, J. Forrer, and M. K. Bowman. We also thank D. van Ormondt and R. de Beer for making the LPSVD program available for us.

Registry No. **1**, 132017-47-1; **2**, 132017-48-2; **3**, 132017-49-3; Di-Boc-L-histidine, 132017-50-6; tris(2-aminoethyl)amine, 4097-89-6; 1,3,5-tris(aminomethyl)benzene, 77372-56-6; Boc-L-methionine, 2488-15-5.

(37) Hathaway, B. J.; Billing, D. E. *Coord. Chem. Rev.* **1970**, *5*, 143.
(38) Palmer, M. H.; Scott, F. E.; Smith, A. S. *Chem. Phys.* **1983**, *74*, 9.
(39) In order to unambiguously differentiate between these two structures additional ESEEM experiments, with deuterated methanol and deuterated acetate, determining the number of the oxygenous ligands, should be carried out.
(40) Laussac, J.-P.; Robert, A.; Haran, R.; Sarker, B. *Inorg. Chem.* **1986**, *25*, 2760.